9
Proportional chambers

Proportional chambers are particle detectors consisting essentially of a container of gas subjected to an electric field. A passing particle can leave a trail of electrons and ions in the gas. The charged particle debris are collected at the chamber electrodes and in the process provide a convenient electrical signal, indicating the passage of the particle. The detector operates as a proportional chamber when the applied electric field is large enough so that the accelerated electrons cause secondary ionization, yet small enough so that the output pulse is still proportional to the number of primary ion pairs. Multiwire proportional chambers are widely used for particle tracking and for triggering.

9.1 Elements of a proportional chamber

The essential elements of a proportional chamber can be illustrated by the apparatus shown in Fig. 9.1. The cylindrical chamber is held at ground potential. The anode wire, which runs along the axis of the cylinder, is maintained at high voltage and is electrically insulated from the cylinder. The electric field inside the chamber is

$$\mathscr{E} = \frac{V_0}{r \ln(r_c/r_w)} \tag{9.1}$$

where r_c is the radius of the cylinder and r_w is the radius of the anode wire. The interior of the cylinder contains a gas such as argon. The chamber has a capacitance per unit length of

$$C = \frac{2\pi\epsilon}{\ln(r_c/r_w)} \tag{9.2}$$

where ϵ is the dielectric constant of the chamber gas. A typical value of C is around 9 pF/m.

https://doi.org/10.1017/9781009290098.010 Published online by Cambridge University Press

Figure 9.1 Basic elements of a proportional counter.

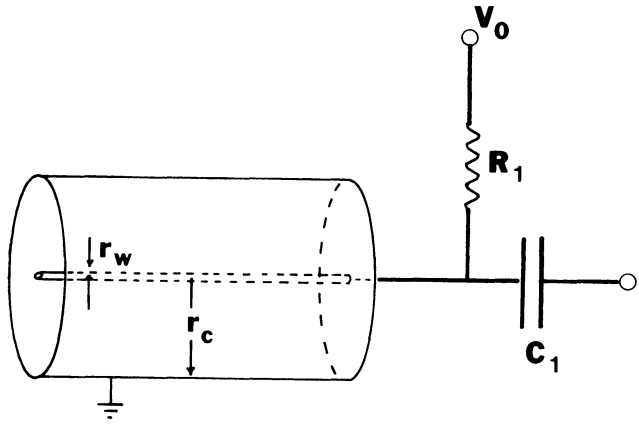

Figure 9.2 Number of collected ions in a proportional counter versus applied voltage. Regions: (R) recombination, (IC) ionization chamber, (PC) proportional chamber, (GC) Geiger counter, (D) continuous discharge. The upper (lower) curve is for a heavily (minimum) ionizing particle.

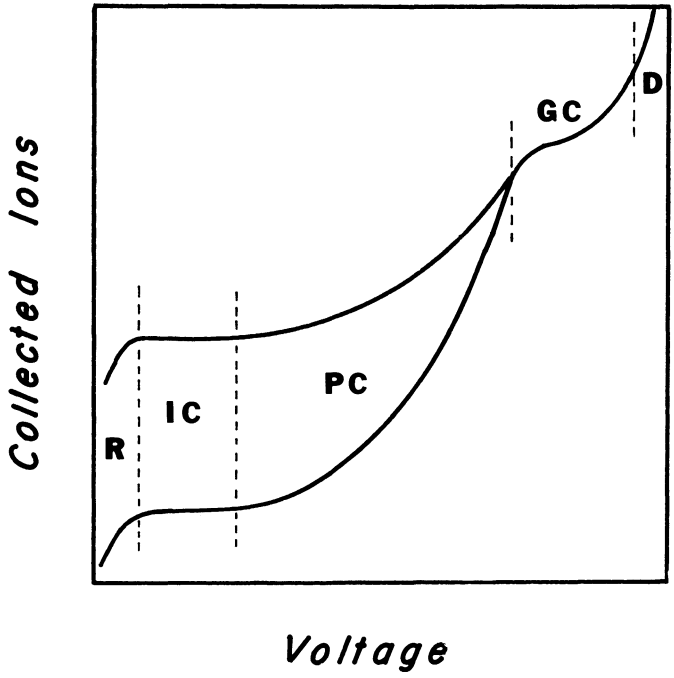

https://doi.org/10.1017/9781009290098.010 Published online by Cambridge University Press

The passage of a charged particle through the gas liberates electron – ion pairs. Typically 30 eV is lost for every ion pair that is formed. As the liberated charges migrate toward the electrodes, they induce a signal in the external circuit. The magnitude of the induced voltage signal is given roughly by

$$V = \frac{MNe}{CL} \tag{9.3}$$

where N is the number of created ion pairs, M is the multiplication factor that takes into account the additional electron – ion pairs created by secondary ionization, and L is the length of the chamber. Because of the $1/r$ field dependence, most of the secondary ionization occurs within a few wire diameters of the anode.

The voltage characteristics of this type of chamber are shown in Fig. 9.2. At very low voltages some of the ions recombine before they can be collected by the electrodes. In the second region all of the ionization products are collected by the electrodes, but the accelerated charged particles do not have sufficient energy to cause secondary ionization. In this region the chamber operates as an ionization counter. Unfortunately, the signal is extremely small. Ionization counters are useful in an integrating mode in high flux environments, for example as beam monitors. As the voltage is increased, the electrons acquire sufficient energy to cause secondary ionization. Here the signal is proportional to the initial ionization, yet is amplified over the signal from an ionization chamber. At higher voltages the chamber enters the Geiger mode, where the signal is very large, but independent of the initial ionization. Finally above a certain voltage the chamber continuously discharges, independent of external conditions.

The signal induced on the anode wire receives contributions from the flow of electrons and positive ions [1 – 3]. Consider a particle with charge Q moving in the electric field. The work the charge performs in moving through a potential drop ΔV is $Q\,\Delta V$. This energy is replenished by the external circuit, which supplies a charge ΔQ_a to the anode to keep the applied voltage constant. Thus, we must have

$$Q\,\Delta V = V_0\,\Delta Q_a$$

and the voltage signal induced on the anode ΔV_a can be written

$$\Delta V_a = \frac{Q}{LCV_0}\frac{dV}{dr}\,dr \tag{9.4}$$

The induced voltage is seen to depend on the potential drop through

https://doi.org/10.1017/9781009290098.010 Published online by Cambridge University Press

which the particle moves. Since all the multiplication takes place very close to the anode wire, most of the electrons only move through a very small potential drop. Most of the positive ions, on the other hand, must cross almost the entire electrode gap, so they experience the full potential drop of the chamber. As a result, under typical proportional chamber conditions, the anode signal is almost entirely due to the motion of the positive ions.

9.2 Fundamental processes in gases

Before we discuss the properties of proportional chambers in more detail, it is important to understand the types of processes that can occur in a gas subjected to an electric field. A particle traversing a gaseous medium loses energy by elastic scattering, by excitation, and by ionization of the gas atoms or molecules. The energy loss of the incident particle in elastic scattering is generally so small that it does not play a significant role in the operation of gaseous detectors. The excitation process raises the gas atoms or molecules to an excited energy level, subject to the selection rules for transitions among the energy levels [4]. The atoms deexcite by photon emission. Formation of a meta-stable state is also possible if direct transition to the ground state is forbidden.

The most important process for the operation of gaseous detectors is ionization. In this case one or more electrons are liberated from the atoms of the medium, leaving positive ions and electrons. Ionization can occur when the energy imparted to the atom exceeds the ionization potential of the gas. The ionization cross section rises sharply from threshold to a peak and then decreases with increasing energy of the incident particle. Ionization cross sections for electrons incident on the noble gases peak for electron energies around 100 eV [2, 4]. Ionization potentials for some gases are given in Table 9.1. The first ionization potential is the energy necessary to remove an electron from a neutral atom or molecule. The second ionization potential is the additional energy necessary to remove a second electron, thereby leaving a doubly charged ion.

The primary ionization is defined to be the number of ionizing collisions per unit length suffered by the incident particle. Some of the ionized electrons (delta rays) may have sufficient energy to cause still more ionization. Thus, a second quantity, the total specific ionization, defined to be the total number of ions actually created per unit length, is also useful. Values of these quantities for several gases are included in Table 9.1. Notice that the average energy lost in creating an ion pair is roughly 30 eV.

Table 9.1. *Ionization properties of gases*

Gas	First ionization potential (eV)	Second ionization potential (eV)	Primary[a] ionization (cm^{-1})	Total specific[a] ionization (cm^{-1})
H_2	15.4	—	5.2	9.2
He	24.6	54.4	4–6	8–11
N_2	15.5		10–19	56
O_2	12.2		22	73
Ne	21.6	41.1	12	39
Ar	15.8	27.6	29	94–110
Kr	14.0	24.4	~22	192
Xe	12.1	21.2	44	307
CO_2	13.7		~34	91
CH_4	13.1		16	53
C_4H_{10}	10.8		~46	195

[a] For minimum ionizing particle at 1 atm pressure.
Source: Handbook of Chemistry and Physics, 64th ed., Boca Raton: CRC Press, 1983; P. Rice-Evar *Chambers,* London: Richelieu, 1974; F. Sauli, CERN Report 77-09, 1977.

https://doi.org/10.1017/9781009290098.010 Published online by Cambridge University Press

Since the number of collisions that occurs is a statistical process, the primary ionization follows a Poisson distribution. The total specific ionization, on the other hand, is influenced by the production of delta rays, which can result in large secondary ionization. Here the appropriate frequency distribution is that due to Landau or one of its later modifications, which has a significant tail for large ionization. The statistical distributions for primary ionization and total specific ionization have been measured using a streamer chamber with a variable high voltage delay [5]. The measured distribution of streamers (see Section 12.4) confirmed that the primary ionization had a Poisson distribution and that the total specific ionization had a Landau distribution.

Further ionization can occur in certain gas mixtures from the deexcitation of a meta-stable atom. In certain cases the surplus energy can ionize a second atom, a process known as the Penning effect [2]. As an example, consider a mixture of neon and argon. Two of the $2s$ states of neon are meta-stable and can deexcite via collisions with argon atoms. The exited state energy of neon exceeds the ionization potential for argon, and thus the neon can deexcite by ionizing the argon.

$$\mathrm{Ne}^* + \mathrm{Ar} \rightarrow \mathrm{Ne} + \mathrm{Ar}^+ + \mathrm{e}^-$$

The peak fraction of energy lost by an electron due to ionization can in some cases be almost doubled by the addition of 0.1% of argon to the original neon gas [2].

Once the ion pairs have been created in the gas, a number of processes may take place, including recombination, attachment, charge exchange, and absorption by the chamber walls. Positive and negative ions can recombine into neutral atoms or molecules via the process

$$\mathrm{X}^+ + \mathrm{Y}^- \rightarrow \mathrm{X} + \mathrm{Y} + \gamma$$

Electrons can be removed from the gas by recombination with a positive ion

$$\mathrm{X}^+ + \mathrm{e}^- \rightarrow \mathrm{X} + \gamma$$

Assume that a gas contains equal concentrations n of positive and negative ions. The rate of decrease of ions due to recombination follows the relation [4]

$$dn/dt = -\beta n^2 \tag{9.5}$$

where the recombination coefficient β is a property of the gas. The concentration remaining in the gas a time t after the passage of the ionizing particle is then given by

$$n = n_0/(1 + \beta n_0 t) \tag{9.6}$$

https://doi.org/10.1017/9781009290098.010 Published online by Cambridge University Press

where n_0 is the initial concentration of ions. Values of the recombination coefficient are in the range $10^{-8}-10^{-6}$ cm^3/s for various gases [2]. The values increase with Z among the noble gases.

Another means of removing electrons is by the addition of a gas with a large electron affinity. Table 9.2 lists measured values of the electron affinity for some atoms and molecules. The electron may attach itself to a neutral atom, especially if this results in a closed outer shell.

$$e^- + X \rightarrow X^- + \gamma$$

The intensity of free electrons traversing the gas falls exponentially [2],

$$I_e = I_{e0}\exp(-\eta x) \tag{9.7}$$

where η is called the attachment coefficient. This coefficient depends on the incident particle energy and is strongly affected by the presence of an electric field [1]. Some of the gases for which electron attachment is important include water vapor, oxygen, ethanol, SF_6, CCl_4, and the Freons.

Another process resulting in the elimination of the original positive ions is charge exchange. This occurs when the ionization potential of the ion is greater than that of some molecule mixed with the gas. This is usually a polyatomic gas like ethanol or methylal. The polyatomic gas quenches the ion multiplication by neutralizing the ions of the main chamber gas. It dissipates the ionization energy by dissociating into

Table 9.2. *Electron affinities*

Substance	Affinity[a] (eV)	Boiling point (°C)
Cl	3.613	−34.6
F	3.448	−188
Br	3.363	58.8
O	1.466	−183
H	0.80	−253
NO_2	3.91	21.2
UF_6	2.91	56.2
WF_6	2.74	17.5
SF_6	1.43	−63.8
BF_3	2.65	−99.9
O_2	0.45	−183

[a] For gases at 0 K.
Source: Handbook of Chemistry and Physics, 64th ed., Boca Raton: CRC Press, 1983, p. E-62.

https://doi.org/10.1017/9781009290098.010 Published online by Cambridge University Press

smaller fragments and absorbs photons emitted in the radiative deexcitation process.

Proportional chambers use an electric field in the active region of the chamber. The charged ionization products in the gas have a net motion in the direction of the field. The drift velocity of an ion w^+ is related to the strength of the electric field $\mathscr{E}$ through the relation

$$w^+ = \mu^+ \mathscr{E} \tag{9.8}$$

where μ^+, the mobility, is a characteristic of the gas, which can depend on the pressure P and electric field strength. The mobility is inversely proportional to the gas pressure at constant temperature. The mobility of an ion is roughly constant for a restricted range of the variable $\mathscr{E}/P$. This result is a consequence of the fact that for moderate electric fields, the average energy of the ions is only slightly increased by the field [1]. For example, the mobility of Ar^+ ions in argon at 0°C and 1 torr is 1200 cm/s per V/cm for $\mathscr{E}/P \lesssim 40$ V/cm-torr [4]. For larger values of $\mathscr{E}/P$ the drift velocities of many ions are roughly proportional to $(\mathscr{E}/P)^{1/2}$.

Although ions and atoms suffer a large fractional energy loss in their collisions with other atoms, electrons lose energy slowly. As a result, electrons can reach large velocities between collisions. The drift velocity for electrons is shown in Fig. 9.3 for several gases. In general, the electron mobility is a complicated function of $\mathscr{E}/P$. At high fields the drift velocity is typically 5 cm/μs, which is roughly 1000 times faster than the velocity of the heavier ions under similar conditions. The drift velocity is also influenced by the presence of a magnetic field. In the case where both an electric and a magnetic field are present, the electrons drift with a reduced velocity and at an angle with respect to the electric field (see Appendix F).

An assembly of ions will diffuse from a region of high concentration to a region of low concentration. The fraction of the original number of ions N_0 present after a time t in the interval of distance dx at x is given by [1]

$$dN/N_0 = (4\pi Dt)^{-1/2} \exp(-x^2/4Dt)\, dx \tag{9.9}$$

where D is the diffusion coefficient. This equation indicates that the ions are spread out with a Gaussian distribution, whose width increases rapidly with time. The diffusion coefficient can depend on the value of the electric field. Electrons diffuse more than ions because of their larger mean free path and higher thermal velocity. Generally the motion of ions or electrons in one dimension will be dominated by the electrical force. Motion perpendicular to the drift direction will be determined by diffusion. The radius of the distribution in two dimensions after a time t is given by [2]

$$\langle r^2 \rangle = 4Dt \tag{9.10}$$

The amount of diffusion is also affected by the presence of a magnetic field. The electrons spiral around the magnetic field lines with the consequence that if the field is sufficiently high, the diffusion perpendicular to B is reduced.

If some region contains a nonuniform concentration of ions of either charge, there will be an additional contribution to the motion due to the electrostatic space charge repulsion. The charge density ρ varies with time according to the relation [4]

$$-\partial\rho/\partial t = \nabla \cdot (\rho w) \tag{9.11}$$

where w is the drift velocity.

Now let us consider the processes leading to an electric current through the gas. The passage of the ionizing particle frees many pairs of electrons and ions. If no electric field were present, the ions and electrons would diffuse and in the process collide with other atoms and molecules in the gas. After traveling several mean free paths, the electrons can reach a thermal velocity of $\sim 10^7$ cm/s under typical conditions. The thermal velocity of positive ions, on the other hand, is only $\sim 10^5$ cm/s on account of their much larger mass. If an electric field is present in the gas, a net drift velocity toward the electrodes is superimposed on the thermal motions. If

Figure 9.3 Electron drift speeds in methane, ethane, and ethylene. (After B. Jean-Marie, V. Lepeltier, and D. L'Hote, Nuc. Instr. Meth. 159: 213, 1979.)

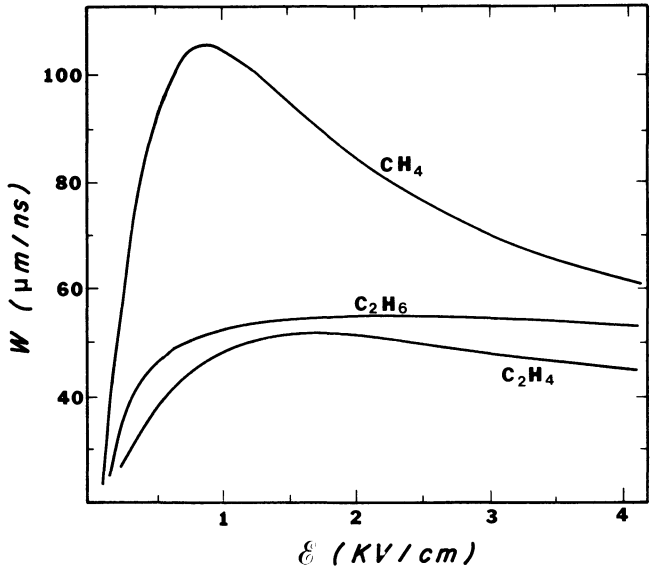

https://doi.org/10.1017/9781009290098.010 Published online by Cambridge University Press

the field is high enough, the electrons can reach sufficient energies to cause secondary ionization. The number of electrons can continue to multiply until an avalanche of $\sim 10^8$ electrons is formed. At this point space charge repulsion may prevent further growth.

The number of electrons produced by a single electron traveling 1 cm along the field is known as Townsend's first ionization coefficient α. Note that α^{-1} is the electron mean free path for ionization in the gas. Values of α are given approximately by

$$\alpha/P = A \exp(-BP/\mathscr{E}) \tag{9.12}$$

where P is the pressure, $\mathscr{E}$ is the applied electric field, and A and B are constants. Table 9.3 lists values of A and B for various gases. Many gases have a peak value of α/P of about 8 ion pairs/cm-torr.

Consider a gas confined in the space between two parallel electrodes a distance d apart, as shown in Fig. 9.4. Suppose that an ionization event occurs at a distance x from the anode. Under proportional chamber conditions the total number N of free electrons grows as they are swept onto the anode. The change in the number of electrons after traveling a distance between y and $y + dy$ is

$$dN = \alpha N \, dy$$

and the total electron multiplication over the distance x is

$$M(x) = e^{\alpha x} \tag{9.13}$$

If the electric field is not uniform, α will be a function of x, and the total

Table 9.3. *Values of the* A *and* B *coefficients for gases*

Gas	A (cm^{-1} $torr^{-1}$)	B (V/cm torr)	Range of validity for $\mathscr{E}$/P (V/cm torr)
H_2	5	130	150–600
N_2	12	342	100–600
CO_2	20	466	500–1000
H_2O	13	290	150–1000
He	3	34	20–150
Ne	4	100	100–400
Ar	12–14	180	100–600
Kr	17	240	100–1000
Xe	26	350	200–800

Source: P. Rice-Evans, *Spark, Streamer, Proportional and Drift Chambers,* London: Richelieu, 1974; A. von Engel, *Ionized Gases,* London: Oxford, 1955.

multiplication will be given by

$$M(x) = \exp\left[\int_x^0 \alpha(y)\, dy\right] \tag{9.14}$$

An actual electron avalanche resembles a teardrop with the electrons highly concentrated at the leading edge [1]. The positive ions are present throughout the entire region occupied by the avalanche. Since their drift velocity is a factor of 10^3 smaller than the electron drift velocity, they slowly diminish in concentration away from the leading edge.

Several effects can lead to modifications of Eq. 9.14. Positive ions striking the cathode can liberate additional electrons. In addition, energetic photons emitted anywhere in the gap may strike the cathode and produce electrons via the photoelectric effect. These processes cause an increase in the current. An opposite effect occurs if the gas is effective in attaching electrons.

The coefficient α can be used to predict the onset of discharge in a chamber. According to the Raether condition, breakdown occurs when [1]

$$\alpha d \gtrsim 20$$

where d is the electrode separation. Notice that increasing the electrode separation for constant α increases the probability of a breakdown.

Figure 9.4 Ionization in the gap between parallel plate electrodes.

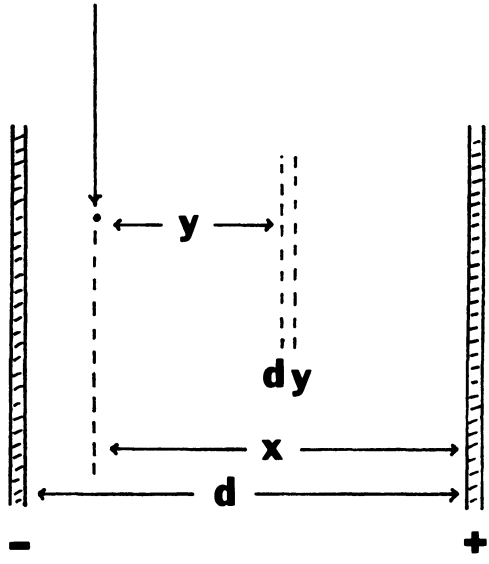

https://doi.org/10.1017/9781009290098.010 Published online by Cambridge University Press

9.3 Proportional chamber gases

A large number of gases have been investigated for use in proportional chambers. Desirable properties of the gas include low working voltage, high gain, good proportionality, high rate capability, long lifetime, high specific ionization, and fast recovery [1]. It is necessary to use mixtures of gases to optimize as many desirable features as possible. The main gas component is usually chosen to be argon, since it has a large multiplication at a relatively low working voltage, has a high total specific ionization, and is economical. Pure argon chambers are limited to gains $\sim 10^3$ since the photons emitted in the deexcitation of excited argon atoms can cause secondary emission at the cathode. For this reason, a polyatomic gas is usually mixed with the argon.

Excited polyatomic molecules have many rotational and vibrational levels. Examples of some commonly used gases are Freon, CO_2, and isobutane. These gases absorb photons over a wide range of energies, and they deexcite through elastic collisions or dissociation into simpler molecules. Secondary emission is also unlikely when ionized polyatomic molecules are neutralized at the cathode. Mixtures of argon with a gas of polyatomic molecules are capable of achieving gains ($\sim 10^6$) much higher than pure argon.

Still higher gains ($\sim 10^7$) can be obtained with the addition of a small amount of an electronegative gas, such as Freon or ethyl bromide. A particular gas mixture in common use ("magic gas") consisting of argon, isobutane, and Freon-13 B1 roughly in the proportion 70/29.6/0.4 gives amplifications of 10^8. Unfortunately, the dissociation products of the isobutane can recombine to form solid or liquid residues that contaminate the chamber electrodes [2]. Positive space charge can build up on this layer for high rate operation and cause serious distortions of the electric field. Some other characteristics of high rate operation are a drop-off of signal size and efficiency, an increase in singles counting rate (noise), and a decrease of the extent of the high voltage operating plateau [1]. This aging process can be reduced by adding a fourth, nonpolymerizing gas, such as methylal, $CH_2(OCH_3)_2$, into the mixture. It is advantageous to work with lower gains if suitable low noise readout electronics is available. Problems associated with chemical deposition on the wires, broken wires, and spark breakdown are all reduced in low gain operation.

Behrends and Melissinos [6] have used a simple, single wire proportional chamber to examine properties of argon–ethane and argon–methane gas mixtures. Measurements of the electron multiplication in argon–ethane at 1 atm, due to the irradiation of the chamber with X-rays,

are shown in Fig. 9.5. The multiplication is seen to increase with increasing high voltage and to decrease with increasing ethane concentration. The multiplication M for a given gas composition is found to vary exponentially with high voltage V,

$$M = e^{\gamma(V-V_0)} \tag{9.15}$$

where γ is the slope and V_0 is a threshold voltage. The exponential multiplication was found to be valid for $10^2 < M < 10^4$. The secondary ionization process is limited by space charge when the charge density of positive ions in the vicinity of the wire becomes comparable to the charge on the anode wire. We note from Fig. 9.5 that the slopes of the curves are

Figure 9.5 Electron multiplication as a function of high voltage for mixtures of argon–ethane. (S. Behrends and A. Melissinos, Nuc. Instr. Meth. 188: 521, 1981.)

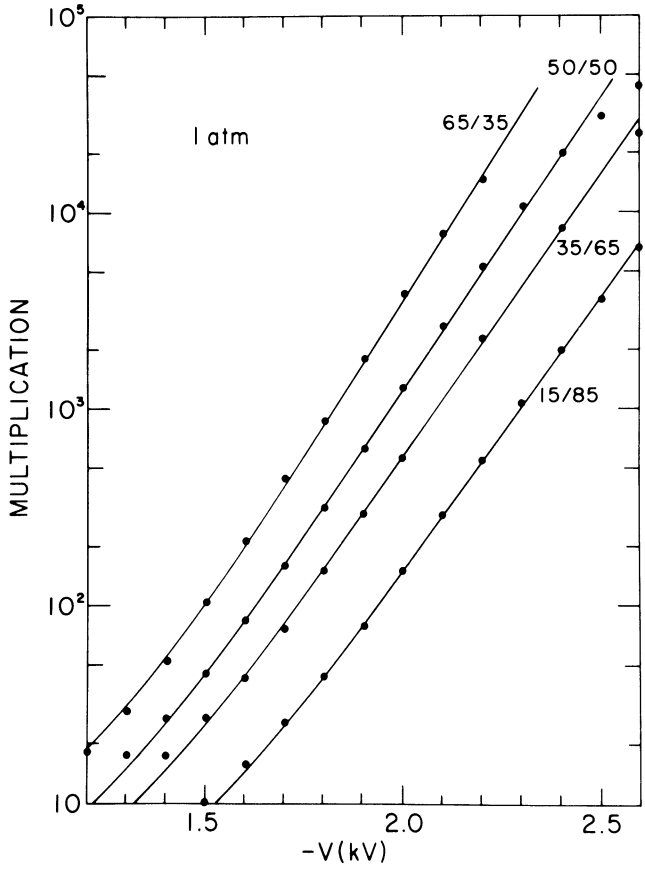

https://doi.org/10.1017/9781009290098.010 Published online by Cambridge University Press

insensitive to the gas composition. Gases with high ethane concentration require a large threshold V_0 before overcoming its quenching ability.

The resolution of the chamber signal was found to be optimum for $M \sim 10^3$. The resolution deteriorates at lower M due to fluctuations in the multiplication process and the stability of the preamplifier gain at low signal levels. The deterioration of the resolution at high multiplication is thought to be due to secondary production of photons, which can photoemit electrons from the cathode. The resolution at high multiplication improves with increasing ethane concentration.

9.4 Multiwire proportional chambers

A very important development in high energy instrumentation was the construction of multiwire proportional chambers (MWPC) by Charpak and his collaborators at CERN [3, 7]. In a MWPC a plane of anode wires is separated from two cathode planes. Each anode wire acts as an individual proportional counter, thereby allowing a big improvement in spatial resolution. These chambers can be used as trigger elements and have shorter deadtime, better resolving time, and higher efficiency than spark chambers. On the other hand, the signal is small, so that independent amplification of each anode is required.

The geometry of a typical chamber is shown in Fig. 9.6. The anode–cathode gap L is usually chosen to be 3 or 4 times the anode wire spacing s [1]. Some typical values for the dimensions are $s = 2$ mm, $L = 8$ mm, and $d = 30\ \mu$m.

In the limit of zero wire diameter the potential in a chamber with anode wires equidistant from cathode planes is [1]

$$V(x, y) = \frac{CV_0}{4\pi\epsilon_0}\left\{\frac{2\pi L}{s} - \ln\left(4\sin^2\frac{\pi x}{s} + 4\sinh^2\frac{\pi y}{s}\right)\right\} \qquad (9.16)$$

Figure 9.6 Geometry of a multiwire proportional chamber.

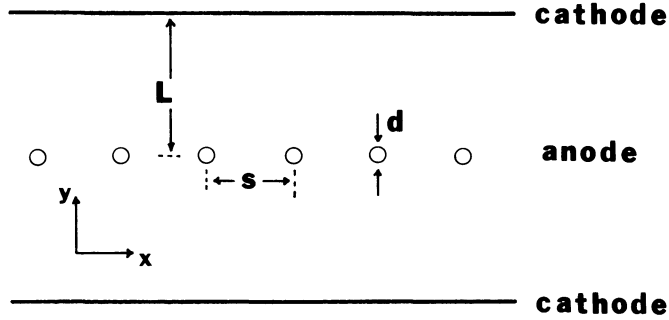

https://doi.org/10.1017/9781009290098.010 Published online by Cambridge University Press

where V_0 is the potential at the anode wires and $V = 0$ at the cathodes. The equipotential lines are approximately circular near the anode wires and planar several wire spacings from the anode plane. The potential for cathode planes consisting of separated cathode wires is more complicated and may deviate significantly from Eq. 9.16 for large cathode wire spacings [8]. The capacitance per unit length is given by

$$C = \frac{2\pi\epsilon_0}{\pi L/s - \ln(\pi d/s)} \tag{9.17}$$

where d is anode wire diameter. The capacitance per unit length of the typical chamber mentioned above is 3.56 pF/m.

The electric field distribution is shown in Fig. 9.7. For most of the time following the creation of an electron–ion pair, the electron merely drifts in the field. Almost all the secondary ionization occurs within several wire diameters from the anode, where the electric field goes as $1/r$. As a result, the amount of multiplication is a strong function of the wire diameter. Thick wires have a very steep gain versus voltage dependence [1]. On the other hand, the wire diameter must not be too small or else it would be incapable of maintaining the tension necessary to resist the electrostatic forces acting on the wire.

Measurements of the avalanche distribution in a MWPC operating in the proportional regime have shown that the avalanche is localized to one

Figure 9.7 Typical electric field pattern in a MWPC (solid lines); equipotential surfaces (dotted lines).

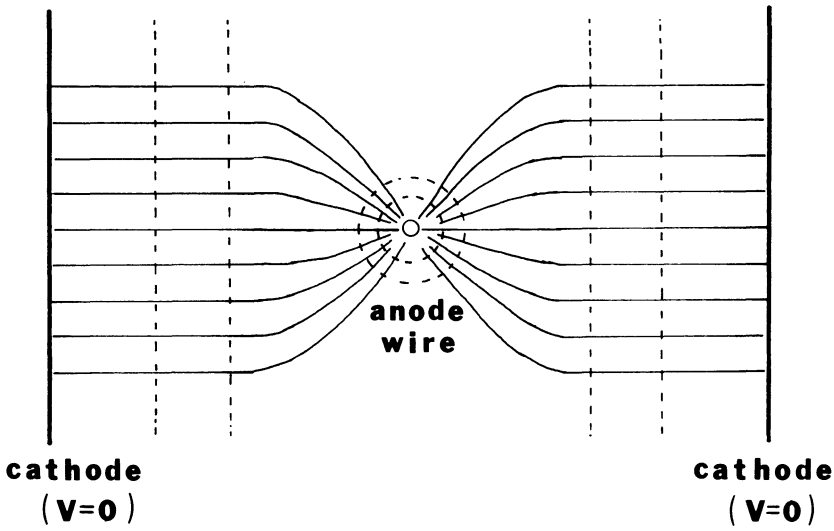

side of the anode wires [9]. However, as the collected charge is increased above 10^7 equivalent electrons, the avalanche begins to surround the wire. Under normal conditions the avalanche is also localized along the wire to within 0.5 mm [1].

The negative pulse on the anode wire induces positive pulses on its neighboring wires, although for $s = 2$ mm the induced signals are only about 20% the size of that on the active wire. There is also a complementary pulse induced on the cathode [3].

Sometimes it is desirable to operate the chamber in the saturated gain regime. Magic gas is frequently used in this way. Under these conditions the anode pulse height is almost independent of the energy lost by the incident ionizing particle. Although the chamber has no energy resolution, it is highly efficient, and the large amplitude and reduced dynamic range of the output pulses simplifies the readout electronics.

It is important that the wire spacing be very uniform throughout the detector. A small displacement of a wire or irregularities in the diameters of the wires can lead to a large change in the charge on the displaced wire and on adjacent wires. The wires tend to stagger themselves out of the plane due to electrostatic repulsion. Vinyl-coated support wires perpendicular to the anode wires have been used to prevent this. Mechanical variations can be expected to lead to variations of 30 – 40% in the gain [1].

The voltage V_0 applied to the wires must be such that the electrostatic force on the wire is smaller than the restoring force due to the tension T of the wire, or that [1]

$$V_0 \leq \frac{s\sqrt{4\pi\epsilon_0 T}}{LC} \tag{9.18}$$

where L is the length of the wire, s is the wire spacing, and C is the capacitance per unit length. The breaking strength available depends strongly on the wire diameter. For example, for 5-μm-diameter tungsten wires a tension up to 0.04 N can be used, while for 30-μm wires this increases to 1.45 N. Electrostatic forces also cause a net attraction of the cathode electrodes toward the anode plane. This can cause a variation of the gap separation across the chamber and is another cause of gain variation.

The high voltage power supply used with the chamber should be equipped with circuitry to shut off the voltage and discharge the chamber when a sudden surge of current is detected. Otherwise the stored energy in the circuit may cause a gap that breaks down to arc repeatedly, with the danger that a wire may break.

Detailed descriptions of all aspects of chamber construction can be found in the latest proceedings of the International Wire Chamber Conference [10]. For the sake of illustration we will describe here some details of the construction and performance of two actual chambers. Crittenden et al. [11] constructed a set of 1-mm pitch MWPCs capable of operating at high rates. A cross section of one edge of the chamber is shown in Fig. 9.8. Each chamber contained a plane of vertical anode wires with a 1-mm separation and two planes of anode wires with 2-mm spacing oriented $\pm 45°$ from the vertical. The anode wires were 15-μm-diameter gold-plated tungsten, tensioned to 25 g and glued onto a G-10 frame. The chamber was desensitized in the beam region by attaching a small piece of Mylar to the anode wires. Cathode planes were located 3.2 mm on either side of the anode plane. The cathodes were made of stainless steel wire cloth with a wire diameter of 50 μm and a spacing of 0.5 mm. The modules were held in an aluminum frame using RTV silicone rubber to form the gas seal. Alignment pins were used so that it was possible to accurately reassemble the chamber. The gas was confined in the chamber using heat shrunk Mylar windows.

The gas mixture used with the 1-mm chamber was 58% argon, 25% isobutane, 16% methyal, and 0.6% Freon-13 B1. The efficiency of the chamber for various beam intensities is shown in Fig. 9.9 as a function of the chamber high voltage. At low intensity the efficiency rapidly increases to a wide plateau near 100%. The efficiency at a fixed high voltage drops off as the intensity is increased. The efficiency can be partially restored by increasing the high voltage, although the plateau region becomes nar-

Figure 9.8 Cross section of a high rate MWPC. (R. Crittenden, S. Ems, R. Heinz, and J. Krider, Nuc. Instr. Meth. 185: 75, 1981.)

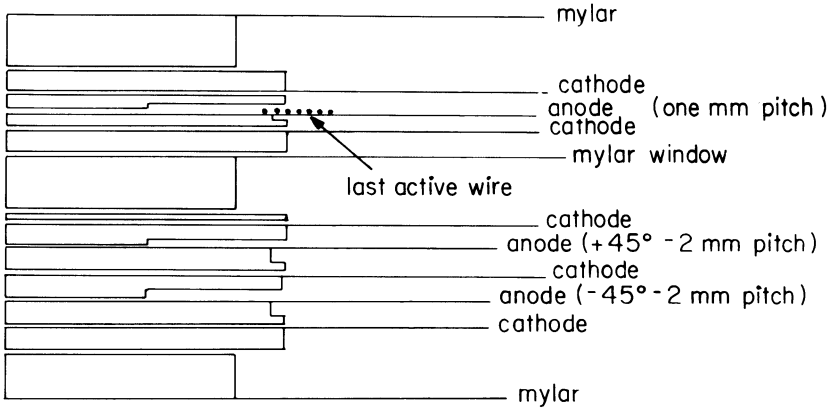

https://doi.org/10.1017/9781009290098.010 Published online by Cambridge University Press

rower. The efficiency at a given high voltage is also strongly dependent on the gas composition.

A set of large (~ 8 m^2) MWPCs were built for the NA3 Spectrometer at the SPS [12]. The chambers were required to handle a large particle flux and to have good efficiency for multitrack events. The anodes were made of 20-μm-diameter gold-plated tungsten. The cathodes consisted of 25-μm-thick plastic foils coated with graphite. The cathode surface was subdivided electrically so that the beam region of the chamber could be desensitized for high rate running. The electrodes were strung over a reinforced epoxy frame, which was accurately pinned into a steel support frame. The aluminized Mylar chamber windows were glued to the steel frame. The long chamber wires were stabilized against electrostatic forces using zigzag-shaped pieces of plastic called garlands.

MWPCs have nearly 100% efficiency for the detection of single, minimum ionizing particles. Because each of the wires is essentially an independent detector, the efficiency for detecting many simultaneous tracks is also very high. Among the more important factors affecting the efficiency are the specific ionization of the gas, the pathlength in the chamber, the high voltage, the angle of incidence of the ionizing particle, and the

Figure 9.9 Particle detection efficiency as a function of high voltage and incident particle rate for the chamber of Fig. 9.8. (R. Crittenden, S. Ems, R. Heinz, and J. Krider, Nuc. Instr. Meth. 185: 75, 1981.)

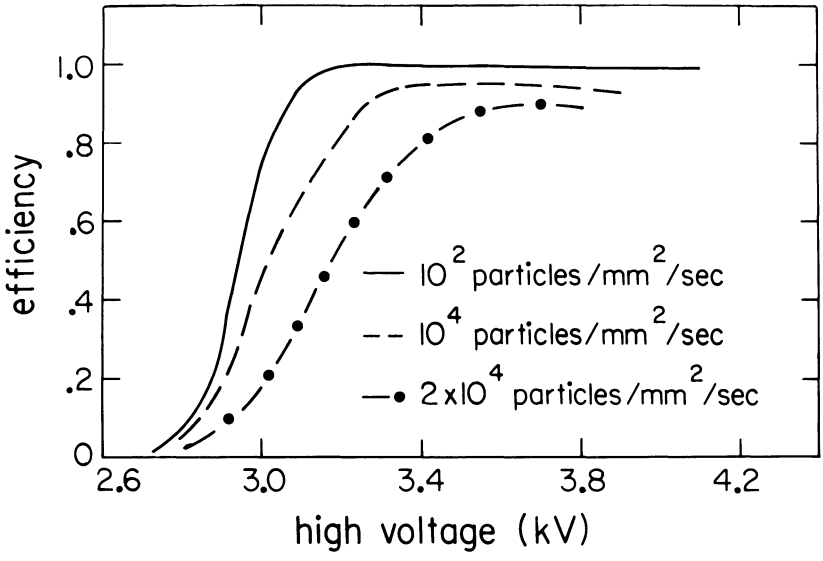

https://doi.org/10.1017/9781009290098.010 Published online by Cambridge University Press

width of the timing gate for accepting pulses after the ionizing particle has passed [3].

The spatial resolution of a MWPC is on the order of half the wire spacing. Improving the spatial resolution by decreasing the anode spacing below 2 mm is difficult because, according to Eq. 9.17, this decreases the capacitance per unit length. Thus, to maintain a fixed gain, the voltage must be correspondingly increased, thereby diminishing the stability of the chamber operation. The spatial resolution can be significantly improved by segmenting and reading out the signal on the cathode. This is discussed further in the following section. With analog readout the resolution can approach the ultimate localization accuracy of the chamber determined by the physical extent and distribution of ionization clusters and the diffusion of the produced charges before they are collected.

Tracks inclined at large angles will fire a cluster of wires [3]. This can be seen in Fig. 9.10, which shows that a 40° track can fire six or seven adjacent wires. The effect can be minimized at the cost of some loss of efficiency by the addition of an electronegative gas such as ethyl bromide. This reduces the sensitive region to a small cylinder around the wire. Alternatively, the timing gate could be shortened so that only pulses from

Figure 9.10 Wire cluster size as a function of the direction of the incident particle. (G. Charpak, reproduced with permission from the Annual Review of Nuclear Science, Vol. 20, © 1970 by Annual Reviews, Inc.)

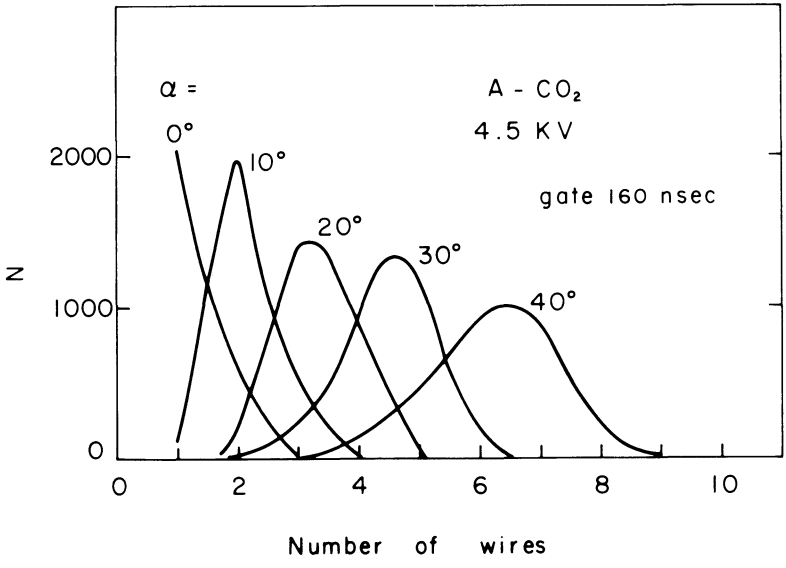

https://doi.org/10.1017/9781009290098.010 Published online by Cambridge University Press

electrons liberated near the wire would be accepted or by only accepting the first pulse to arrive. Production of delta rays also leads to large clusters.

The uncertainty in the arrival time of a pulse at the logic electronics after the passage of an ionizing particle is the time resolution of the chamber. A value of around 30 ns is typical for 2-mm wire spacing. The actual arrival time of the pulse is correlated with the position at which the track crosses the chamber. A typical distribution of time delays on a single wire consists of a large peak arising from tracks that pass within several wire diameters of the wire and a long tail from electrons produced outside this region. The time resolution may be improved at the expense of some inefficiency by the addition of an electronegative gas. Another technique is to use several chambers with the wire spacings staggered, so that the wires of the second chamber are behind the interwire gap of the first chamber. Using the first pulse to arrive from any of the chambers reduces the time jitter.

An anode wire is dead for a period of several hundred nanoseconds following a pulse [2]. The actual deadtime depends on the wire spacing and amplifier electronics. During this time the electrons are collected, the positive ions drift away from the region of the anode, and the amplifier circuit recovers.

Figure 9.11 Effect of magnetic field on the counting rate of several adjacent MWPC wires. (After G. Charpak, D. Rahm, and H. Steiner, Nuc. Instr. Meth. 80: 13, 1970.)

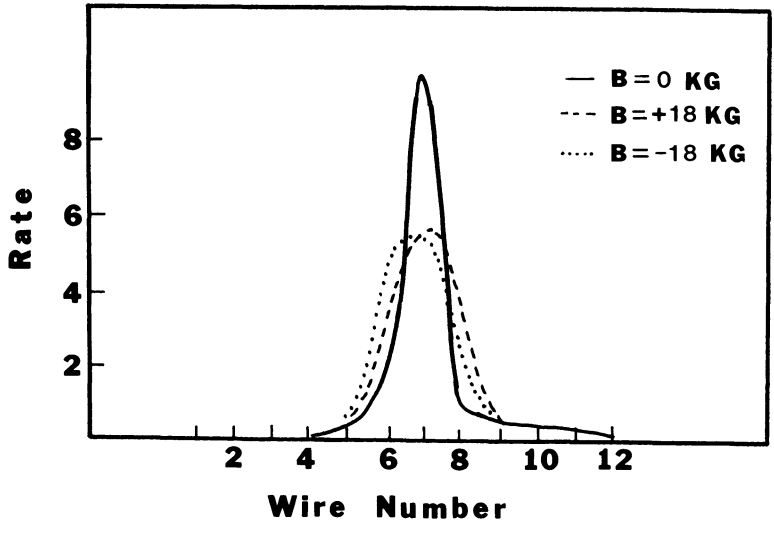

https://doi.org/10.1017/9781009290098.010 Published online by Cambridge University Press

When a MWPC is operated inside a magnetic field oriented parallel to the anode wires, the electrons drift in the direction $\mathscr{E} \times B$ before they are collected at the anode wire. However, the drift is in opposite directions for ions produced on opposite sides of the central wire plane. As a result, if the readout electronics is sensitive to the start of the ionization pulse, the mean of the collected charge distribution is not very sensitive to B [7]. This can be seen in Fig. 9.11, which shows the counting rate on 12 adjacent wires as the magnetic field is varied. Note that the rate on the central wire decreases as the field is increased, but the rate on the adjacent wires increases with the result that the total counting rate remains constant. Thus, the magnetic field only gives a small displacement and a slight loss of resolution. No effect is observed when the magnetic field is parallel to the electric field.

The MWPC wire arrangement can be modified for operation in very high flux environments. In the multistep avalanche chamber [13] the incident particles first enter a preamplification region. The ionization electrons drift toward a pair of wire meshes, which act as a gate to the second half of the chamber. The potential on the gate can be biased so that all the charge is collected, and no electrons make it to the anodes in the second half of the chamber. During the time the electrons are drifting in the preamplification region, external trigger logic can decide if the particle should be detected. In that case a potential of the opposite polarity is applied to the gate. The major problem with the scheme appeared to be capacitive coupling between the gate meshes and the anode.

9.5 Readout electronics

The task of the readout electronics is to provide sufficient information so that the positions where ionizing particles traversed the chamber may be determined as accurately as possible. The time dependence of the anode signal v can be found by assuming that the signal is totally due to a group of positive ions that leave the surface of the anode wire with constant mobility at $t = 0$ [1]. Integrating Eq. 9.4, we find

$$v(t) = \frac{-Q}{2\pi\epsilon_0 L} \ln \frac{r(t)}{r_w} \tag{9.19}$$

where $r(t)$ gives the distance of the positive ions from the axis of the cylinder. Using the definition of mobility, $r(t)$ can be written

$$r(t) = \left(r_w^2 + \frac{\mu^+ C V_0}{\pi\epsilon_0} t \right)^{1/2} \tag{9.20}$$

https://doi.org/10.1017/9781009290098.010 Published online by Cambridge University Press

Substituting back into Eq. 9.19, we find

$$v(t) = -\frac{Q}{4\pi\epsilon_0 L} \ln\left(1 + \frac{\mu^+ CV_0}{\pi\epsilon_0 r_w^2} t\right) \tag{9.21}$$

This important result shows that the voltage has $\ln(1 + t/t_0)$ time dependence.

The output pulse from the anode has a fast initial rise (~6% of maximum in 10 ns). When used with an RC pulse differentiation network, this allows MWPCs to be used as trigger devices. The total undifferentiated pulse length may be several hundred microseconds. The electrons liberated by the ionizing particle drift through varying distances before reaching the high field region near the anode. Thus, the output pulse is the resultant of many pulses arriving over a period of time and has an approximately linear rise at first.

Under typical proportional chamber conditions the initial deposited energy is amplified by 10^4 or 10^5. Even with this amplification individual amplifiers are necessary for each wire to obtain reasonable signal levels (~1 V). The output pulses deviate from strict proportionality because of fluctuations in the number of initial ion pairs and in the amplification.

The design of the chamber readout electronics is as varied as the design of the chambers themselves. One possible readout arrangement for each wire is shown in Fig. 9.12. The amplified signal from the anode wire is sent to a discriminator with an adjustable threshold. The threshold setting (~0.5 mV) is optimized to reject noise, yet maintain high efficiency. In general, full efficiency is obtained for minimum ionizing particles with a threshold that is about one-tenth the peak amplitude [1]. A loss of effi-

Figure 9.12 Simple readout scheme for an anode wire.

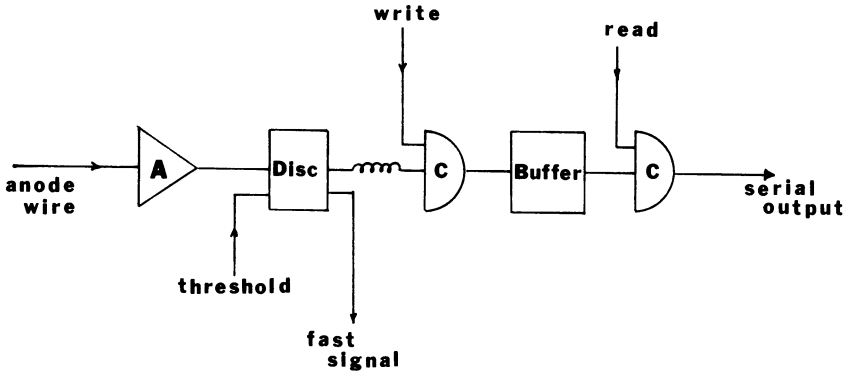

https://doi.org/10.1017/9781009290098.010 Published online by Cambridge University Press

ciency from increasing the discriminator threshold can be offset to some extent by increasing the high voltage.

Following the discriminator a fast signal can be extracted for use in the trigger logic. The signals from all the wires can be combined in order to make multiplicity tests. Another signal from each of the discriminators is then delayed while the trigger decision is being made. For good events the trigger initiates a WRITE signal that allows the anode signals to pass into a buffer. At an appropriate time in the readout cycle, the data handler sends a READ pulse, which allows the signal for each wire to enter the readout data stream. A typical readout scheme would specify the address of one of the hit wires in a cluster and the width of the cluster. Readout electronics systems similar to this are available commercially [14].

A block diagram of the readout electronics for the NA3 MWPCs discussed earlier is shown in Fig. 9.13. The major features of the system include amplifier and readout cards that plug into connectors on the edge

Figure 9.13 Block diagram of the NA3 MWPC readout electronics. (A) amplifier card, (R) readout card, (T) trigger signal, (C) control bus, (D) data bus, (PS) power supply, and (DA) data acquisition system. (After R. Hammarstrom et al., Nuc. Instr. Meth. 174: 45, 1980.)

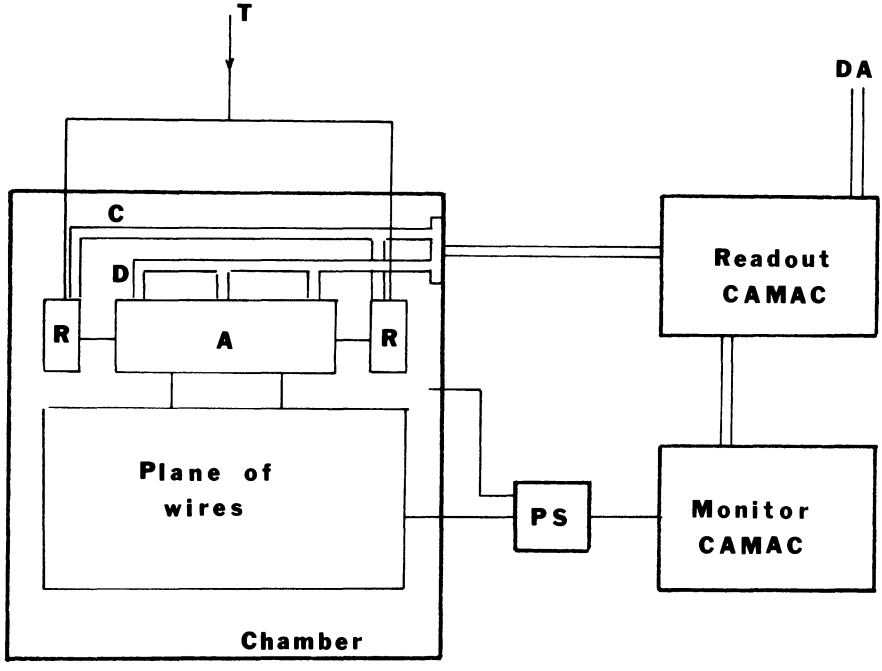

https://doi.org/10.1017/9781009290098.010 Published online by Cambridge University Press

of the chamber, CAMAC modules to enter the MWPC information into the data acquisition system, a computer-controlled power supply system, and a dedicated CAMAC control and monitoring system [12]. The amplifier cards used hybrid integrated circuits that contained differential amplifiers, discriminators, one-shot delays, and an output gate capable of driving the external data bus. The discriminator threshold could be varied from 1 to 10 μA, while the time delay could be adjusted from 330 to 750 ns. During the readout cycle the amplifier card was addressed, causing it to put the contents of the 16 output gates onto the data bus. The data was converted by the CAMAC modules into the corresponding addresses of the hit wires. The readout of a complete chamber plane took about 60 μs.

Improved spatial resolution can be obtained if analog signals from the wires are measured. In this case signals from nearby wires can be averaged in an appropriate manner to interpolate the value of the actual coordinate. The most important analog techniques that have been used for this purpose are listed in Table 9.4. When using these methods, the readout electronics is necessarily more complicated than that shown in Fig. 9.12. The methods listed in Table 9.4 are also used for drift chambers.

Analog signal methods are frequently used to obtain a second coordinate of the particle trajectory without introducing additional planes of wires at different angles. The second coordinate is typically the direction along the anode wire and orthogonal to the particle's trajectory for planar chambers, or the coordinate along the axis for cylindrical chambers.

A common construction uses the amplifier–discriminator readout system mentioned previously for the anode signals and a perpendicular, segmented cathode readout to give the coordinate along the anode wire direction. The cathode strip (or cathode pad) method utilizes the induced charge on a segmented cathode [15]. Chambers with this feature can combine excellent spatial resolution with inherently good time resolu-

Table 9.4. *Analog methods for position measurements in wire chambers*

Method	Requirements
Cathode strips	segmented cathode, each with readout
Delay line	supplementary transmission lines, dual readout
Charge division of anode signal	resistive anode, dual readout
Risetime of anode signal	resistive anode, dual readout
Direct timing of anode signal	high conductivity anode, dual readout

https://doi.org/10.1017/9781009290098.010 Published online by Cambridge University Press

tion. Figure 9.14 illustrates the basic principle. One cathode of the MWPC is segmented perpendicularly to the anode wires. The width of the segments is roughly equal to the anode–cathode separation distance. As the ions are drifting between the electrodes, pulses are induced on nearby cathodes. A charge Q on an anode situated between two cathode planes will induce a charge distribution [16]

$$\sigma(z) = -\frac{Q}{4L} \operatorname{sech} \frac{\pi z}{2L} \tag{9.22}$$

on the perpendicular cathode, where z is the distance along the anode wire and L is the anode–cathode separation. The charge on each cathode pad is measured using an accurate ADC.

The simplest method for determining the position of the particle is to compute the center of gravity

$$\bar{x} = \frac{\sum Q_i X_i}{\sum Q_i} \tag{9.23}$$

of the charges Q_i deposited on the strips [16, 17]. However, the deposited charge must be integrated over the finite width of the strip. This introduces nonlinear correlations and can lead to systematic shifts between the avalanche position and the calculated centroid. Additional nonlinearities may be caused by mutual capacitance between the strips, electronic cross

Figure 9.14 Two-dimensional readout using cathode strips. (A. Breskin et al., Nuc. Instr. Meth. 143: 29, 1977.)

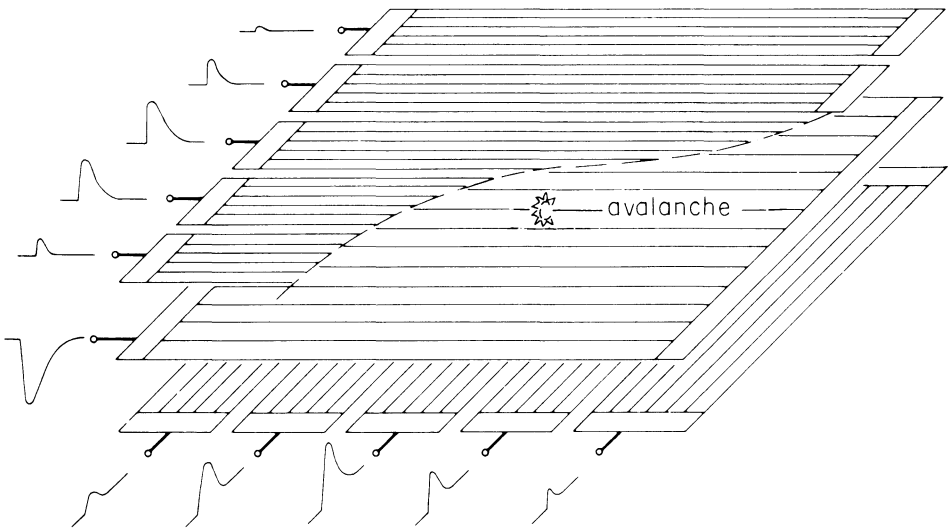

https://doi.org/10.1017/9781009290098.010 Published online by Cambridge University Press

talk, and gain variations between channels. The accuracy of the calculation can be improved by subtracting a bias level from each strip before averaging [17]. Small chambers instrumented with cathode strip readout have achieved 40 μm rms spatial resolution along the anode wires. The resolution is slightly worse for the direction perpendicular to the anode wires.

A delay line is a transmission line that allows the position of a particle to be determined from the difference in arrival times of the signals at the two ends of the line [18]. The delay line may be either tapped directly to the cathode wires, or capacitatively coupled if the signal is sufficiently strong. Delay lines parallel to the anode can limit the rate capability of the chamber.

As an example we mention the drift chambers of the NA-1 Spectrometer at CERN [19]. The chambers used delay lines to provide a measurement of the second coordinate and to aid in the resolution of the left – right ambiguity. The delay lines consisted of 2-mm-diameter aluminum pipe surrounded by Teflon and copper wire. The delay lines ran parallel to the drift chamber sense wires. The signal induced on the delay line propagated with a velocity of 1.6 mm/ns to the edge of the chamber, where a coupling transformer matched the signal to an amplifier. The characteristic impedance was 1800 Ω. The FWHM in the length determination was 4.5 mm.

Analog methods that use the anode signal itself have the advantage of not complicating the chamber construction or introducing additional scattering material. The charge division method determines the position of the avalanche caused by a passing particle by measuring the amount of

Figure 9.15 Principle of the charge division method.

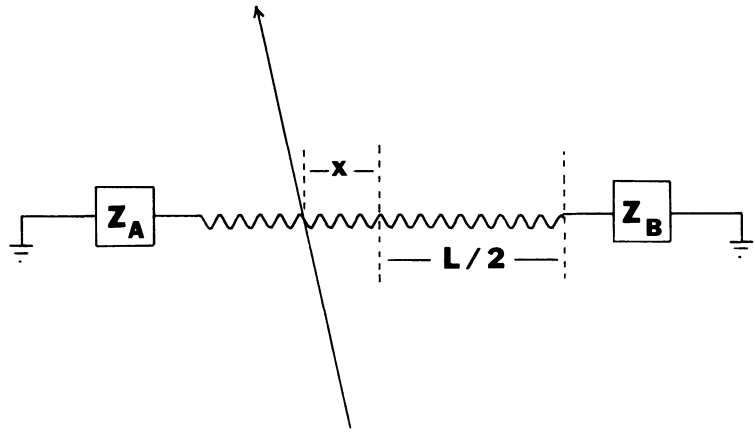

https://doi.org/10.1017/9781009290098.010 Published online by Cambridge University Press

charge reaching the two ends of a resistive wire [20, 21]. Consider a wire chamber constructed with high resistance anode wires of length L as shown in Fig. 9.15. The two ends of the wire are connected to charge sensitive preamplifiers with input impedances Z_A and Z_B. Suppose the avalanche from the passage of a charged particle hits the anode at a distance $\frac{1}{2}L - x$ from the A end. The charges that are induced at the two ends of the wire are inversely proportional to the total impedances along the two paths, so long as the integration time for the signal is long compared to $\rho L C_W$, where ρ and C_W are the resistivity and distributed capacitance of the anode wire. Thus, the ratio of the collected charges is given by

$$\frac{Q_A}{Q_B} = \frac{(\frac{1}{2}L + x)\rho + Z_B}{(\frac{1}{2}L - x)\rho + Z_A} \tag{9.24}$$

It is desirable that the preamplifier input impedances be small compared to the resistance of the wire. The quantities that are actually measured are the ADC channels of the signals. Thus, the position determination may require corrections for any differences in amplifier gain, pedestal corrections, and so on. Resolutions of ~ 0.4 mm have been achieved using charge division [22].

The other two analog methods mentioned in Table 9.4 measure either the risetime of the pulses or the arrival time of the pulses at the two ends of the anode. The readout electronics for the risetime method is simpler than for the charge division method [23]. The method has the disadvantage that it is dependent on all parasitic capacitances and inductances in the chamber and so may not be suitable for large chambers. The direct timing method uses the anode and surrounding electrodes as a delay line [24]. The position of a particle is then determined from the difference of arrival times at the two ends. The resolution of this method is expected to be independent of the length of the wires.

The pulse height of MWPC anode signals have been used to measure the energy loss of particles. This subject will be discussed in the following chapter.

References

A description of the construction and operation of classical ionization, proportional, and Geiger counters can be found in S. Korff, *Electron and Nuclear Counters,* New York: Van Nostrand, 1955.

[1] F. Sauli, Principles of operation of multiwire proportional and drift chambers, CERN Report 77-09, 1977. References to most of the original work on proportional chambers and MWPCs can be found in this and the following reference.

[2] P. Rice-Evans, *Spark, Streamer, Proportional, and Drift Chambers,* London: Richelieu, 1974.

[3] G. Charpak, Evolution of the automatic spark chambers, Ann. Rev. Nuc. Sci. 20: 195–254, 1970.

[4] A. von Engel, *Ionized Gases,* London: Oxford, 1955.
[5] V. Davidenko, B. Dolgoshein, V. Semenov, and S. Somov, Measurements of the relativistic increase of the specific primary ionization in a streamer chamber, Nuc. Instr. Meth. 67: 325–30, 1969.
[6] S. Behrends and A. Melissinos, Properties of argon-ethane/methane mixtures for use in proportional chambers, Nuc. Instr. Meth. 188: 521–34, 1981.
[7] G. Charpak, D. Rahm, and H. Steiner, Some developments in the operation of multiwire proportional chambers, Nuc. Instr. Meth. 80: 13–34, 1970.
[8] S. Beingessner and L. Bird, An extension of the standard formulae for electric fields in MWPCs, Nuc. Instr. Meth. 172: 613–6, 1980.
[9] J. Fischer, H. Okuno, and A. Walenta, Spatial distributions of the avalanches in proportional chambers, Nuc. Instr. Meth. 151: 451–60, 1978.
[10] Proceedings of Wire Chamber Conference, Nuc. Instr. Meth. 176: 1–432, 1980; Nuc. Instr. Meth. 217: 1–381, 1983.
[11] R. Crittenden, S. Ems, R. Heinz, and J. Krider, A design for one mm pitch MWPCs operating at high rates, Nuc. Instr. Meth. 185: 75–9, 1981.
[12] R. Hammarstrom, P. Kristensen, R. Lorenzi, G. Matthiae, A. Michelini, O. Runolfson, J. Timmermans, and M. Uldry, Large multiwire proportional chambers for experiment NA3 at the CERN SPS, Nuc. Instr. Meth. 174: 45–52, 1980.
[13] A. Breskin, G. Charpak, S. Majewski, G. Melchart, G. Petersen, and F. Sauli, The multistep avalanche chamber: A new family of fast, high rate particle detectors, Nuc. Instr. Meth. 161: 19–34, 1979; F. Sauli, Possible improvements in the performance of gaseous detectors, Physica Scripta 23: 526–33, 1981.
[14] For example, the PCOS III MWPC System, LeCroy Research Systems, Spring Valley, NY.
[15] G. Charpak, G. Melchart, G. Petersen, and F. Sauli, High accuracy localization of minimum ionizing particles using the cathode induced charge centre-of-gravity readout, Nuc. Instr. Meth. 167: 455–64, 1979.
[16] I. Endo, T. Kawamoto, Y. Mizuno, T. Ohsugi, T. Taniguchi, and T. Takeshita, Systematic shifts of evaluated charge centroid for the cathode readout proportional chamber, Nuc. Instr. Meth. 188: 51–8, 1981.
[17] G. Charpak and F. Sauli, High resolution electronic particle detectors, Ann. Rev. Nuc. Part. Sci. 34: 285–349, 1984.
[18] E. Beardsworth, J. Fischer, S. Iwata, M. Levine, V. Radeka, and C. Thorn, Multiwire proportional chamber focal-plane detector, Nuc. Instr. Meth. 127: 29–39, 1975.
[19] S. Amendolia, G. Batignani, E. Bertolucci, L. Bosisio, U. Bottigli, C. Bradaschia, M. Budinich, F. Fidecaro, L. Foa, A. Giazotto, M. Giorgi, F. Liello, P. Marrocchesi, A. Menzione, M. Quaglia, L. Ristori, L. Rolandi, A. Scribano, R. Stanga, A. Stefanini, and M. Vincelli, A set of drift chambers built for the FRAMM-NA1 Spectrometer, Nuc. Instr. Meth. 176: 461–8, 1980.
[20] P. Rehak, Detection and signal processing in high energy physics, in G. Bologna (ed.), *Data Acquisition in High Energy Physics,* Amsterdam: North-Holland, 1983, pp. 25–89.
[21] V. Radeka and P. Rehak, Charge dividing mechanism on resistive electrode in position sensitive detectors, IEEE Trans. Nuc. Sci. NS-26: 225–38, 1979.
[22] J. Buskens, B. Koene, L. Linssen, P. Rewiersma, H. Schuijlenburg, R. Van Swol, J. Timmermans, M. Haguenauer, G. Roiron, and J. Velasco. Small high precision wire chambers for the measurement of $\bar{p}p$ elastic scattering at the CERN Collider, Nuc. Instr. Meth. 207: 365–78, 1983.
[23] E. DeGraaf, J. Smits, A. Paans, and M. Woldring, The rise time method for the readout of a proportional chamber: Linearity, sensitivity, and noise, Nuc. Instr. Meth. 200: 311–31, 1982.

[24] R. Boie, V. Radeka, P. Rehak, and D. Xi, Second coordinate readout in drift chambers by timing of the electromagnetic wave propagating along the anode wire, IEEE Trans. Nuc. Sci. NS-28: 471–7, 1981.

Exercises

1. Derive an expression for the radius at which ion multiplication begins in a cylindrical proportional chamber in terms of the applied voltage and the properties of the chamber and of the gas.
2. Use the data of Table 9.3 to estimate the ionization cross for electrons in argon in a 100-V/cm field at 0.5 atm.
3. Derive Eq. 9.12. Use the kinetic theory and assume that any electron whose energy exceeds the ionization potential of the gas will cause ionization.
4. For voltages $V \gg V_0$ the gain factor M can be written $M = ke^{Q}$, where k is a constant and Q is the charge per unit length on the wire. Find the gain variations due to variations in the anode wire diameter, anode wire spacing, and the anode–cathode separation.
5. Estimate the expected signal for a 3-GeV/c proton in a 2-cm-radius proportional chamber containing a 50% Ar/50% C_2H_6 gas mixture at 2000 V.
6. A MWPC with argon gas at atmospheric pressure has $L = 2s$ and 10-μm-diameter anode wires. If the ion multiplication is 10^4, what wire spacing would give 100-mV pulses for minimum ionizing particles?
7. A MWPC has 12-μm-diameter anode wires, 2 mm wire spacing, and 4 mm anode–cathode spacing. Find the critical voltage for wire breakage if the 1-m-long wires are tensioned to 1 N.
8. A 1-m-long wire with resistivity 60 Ω/cm has readout circuits with input impedance 100 Ω at each end. Find the position along the wire of a passing particle if the peak signal is in channel 36 on one side and in channel 20 on the other. Assume the ADC pedestals are in channel 5.